

# Agentic Self-Evolutionary Replanning for Embodied Navigation

Guoliang Li<sup>1</sup>, Ruihua Han<sup>3</sup>, Chengyang Li<sup>3</sup>, He Li<sup>1</sup>, Shuai Wang<sup>2,†</sup>,  
Wenchao Ding<sup>4</sup>, Hong Zhang<sup>5</sup>, *Life Fellow, IEEE*, Chengzhong Xu<sup>1,†</sup>, *Fellow, IEEE*

**Abstract**—Failure is inevitable for embodied navigation in complex environments. To enhance the resilience, replanning (RP) is a viable option, where the robot is allowed to fail, but is capable of adjusting plan until success. However, existing RP approaches freeze the ego action model and miss the opportunities to explore better plans by upgrading the robot itself. To address this limitation, we propose Self-Evolutionary RePlanning, or SERP for short, which leads to a paradigm shift from frozen models towards evolving models by run-time learning from recent experiences. In contrast to existing model evolution approaches that often get stuck at predefined static parameters, we introduce agentic self-evolving action model that uses in-context learning with auto-differentiation (ILAD) for adaptive function adjustment and global parameter reset. To achieve token-efficient replanning for SERP, we also propose graph chain-of-thought (GCOT) replanning with large language model (LLM) inference over distilled graphs. Extensive simulation and real-world experiments demonstrate that SERP achieves higher success rate with lower token expenditure over various benchmarks, validating its superior robustness and efficiency across diverse environments.

**Index Terms**—Cross-level replanning, self-evolution.

## I. INTRODUCTION

Embodied navigation marks a paradigm shift in robotics, aiming to translate natural language task instructions into executable actions [1]. In the case that detailed instructions (e.g., “Walk forward and take left at the sofa.”) are provided, this translation has a high success rate using methods like vision-language navigation (VLN) [2]–[4]. If the task instructions are ambiguous (e.g., “I am thirsty!”), accurate translation can be a formidable challenge. This necessitates large language models (LLMs) [5], [6] for reducing the search space and formulating multi-task strategies [7].

Pioneering LLM-based navigation [8], [9] assume strict plan following, treating each action as feasible and must be succeed. Nonetheless, they can fail in cases when execution failures exist, especially under high environmental uncertainties. To address this issue, replanning (RP) [10]–[14] is a promising solution, where the robot is allowed to fail, but is capable of adjusting plan until success. Current RP methods can be categorized into global-level [10], [11] (i.e., focusing on semantic failure) and local level [12]–[14] (i.e., focusing on physical failure), but there is a lack of attention on joint replanning over both semantic and physical spaces.

Furthermore, an execution failure may be caused by not only external environment uncertainties, but also ego model uncertainties. Existing RP methods [10]–[14] overlook the ego weaknesses and freeze the ego action model during replanning. This may lead the robot to make the same mistakes repeatedly, while circumventing the failure (e.g., seek an easier path)

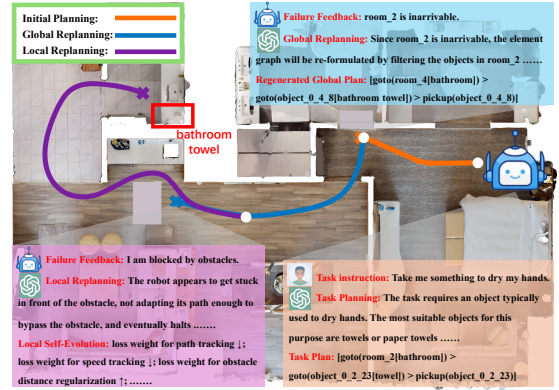


Fig. 1: SERP replans at two-levels with self-evolution.

would introduce additional time cost due to detours. Hence, how to conquer rather than circumvent the failure by upgrading the robot itself becomes an important issue.

To fill the gap, we propose **SERP**, an evolutionary replanning framework that leads to a paradigm shift from frozen models towards evolving models by run-time learning from recent experiences. A replanning example for SERP is illustrated in Fig. 1. The task instruction is: “Find me something to dry my hands.” The robot finds the bathroom towel after a cross-level replanning with run-time self-evolution.

From the above example, we observe two key challenges for realizing SERP. The first one is the difficulties in evolving the action model correctly with closed-loop execution data. In contrast to existing model evolution [15]–[17] that adopts static loss function and often gets stuck at predefined static parameters, we propose an agentic self-evolution (ASE) method, which supports adaptive loss function adjustment and bad optima escape via in-context learning with auto-differentiation (ILAD). The second challenge comes from the repeated LLM inferences over large semantic spaces. This would inevitably introduce excessive token usage and computation latency. To this end, we propose global graph chain-of-thought (GCOT), which distills the original scene graph into a much smaller but semantically relevant graph, by iteratively accumulating the contexts with updated task and execution conditions. Our contributions are summarized as follows:

- Introduce **SERP**, a self-evolving cross-level replanning framework.
- Develop a local-level **ASE** mechanism, enabling run-time model updates by fine-grained ILAD tuning and revealing the mutual assistance between IL and AD.
- Develop a global-level **GCOT** mechanism that maintains a distilled dynamic graph based on task and execution conditions for fast replanning.
- Conduct simulation and real-world evaluations across diverse tasks and environments, demonstrating the superior performance of SERP.

<sup>†</sup> denotes the corresponding authors: s.wang@siat.ac.cn, czxu@um.edu.mo

<sup>1</sup> Department of Computer and Information Science, University of Macau

<sup>2</sup> SIAT, Chinese Academy of Sciences

<sup>3</sup> Department of Computer Science, University of Hong Kong

<sup>4</sup> Academy for Engineering & Technology, Fudan University

<sup>5</sup> Department of EEE, Southern University of Science and Technology

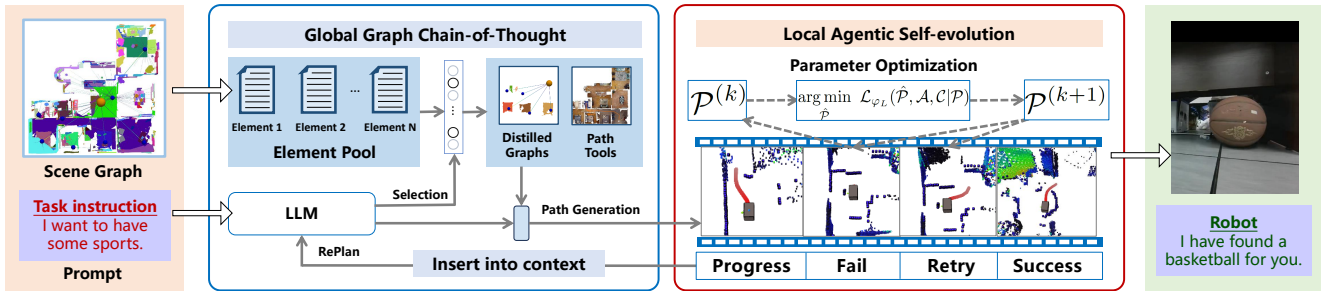


Fig. 2: Overview of SERP, which consists of local agentic self-evolution and global graph chain-of-thought.

## II. RELATED WORK

Embodied navigation interprets natural language instructions and generates executable control commands [1]. Conventional approaches such as semantic parsing [18] and search-based techniques [19] often struggle to generalize across diverse task specifications. Emerging approaches integrate LLM [20]–[23] to interpret complex natural language instructions and generate task plans by exploiting commonsense reasoning. Recent works utilize scene graphs and larger LLMs [9]–[11] to further enhance task generalization. However, they often operate over static topological maps, which restricts adaptability in real environments. To this end, replanning enables the system to reshape plans in response to varying conditions or execution errors. At the global level, iterative LLM-assisted RP has been proposed to verify and refine plans, by exploiting the reasoning capabilities of LLM to infer potential causes of failure [10], [11]. At the local level, existing RP adopt optimization-based strategies [12], [14] or learning-based approaches [13], to reform the trajectories for avoiding dynamic obstacles under perception uncertainties.

Despite these advancements, existing RP methods freeze the ego action model, thereby missing opportunities to identify potentially better plans during the replanning process. To enhance RP, self-evolution is a promising direction, which enables a robot to adapt its internal model, so as to avoid repeated failures in future executions. For instance, recent approaches formulate self-evolution as a gradient-based optimization problem, where system parameters are updated via backpropagation through differentiable models [15]–[17]. However, these self-evolution approaches rely on static loss functions and gradient-only parameter update that may get stuck at a poor local optima. Our ASE method will support adaptive function adjustment and global parameter reset to address their issues.

Existing RP methods also suffer from inefficient LLM utilization, as redundant input may result in excessive token usage in iterative replanning. To reduce the token usage, SayPlan [11] constructs task-relevant subgraph from scene graph. It prompts LLM to identify room-level nodes for expansion, thereby constructing a candidate node pool from which relevant nodes are subsequently selected to form a subgraph. This procedure is executed iteratively until the resultant subgraph is deemed sufficient for task completion. While successfully reducing the graph size, SayPlan costs additional token usage during the graph distillation phase. In contrast, our approach adds a feature matching block between node attributes and

task-relevant objects to retrieve a concise set of semantically relevant candidate nodes. This block utilizes a small contrastive language-image pre-training (CLIP) model instead of an LLM. The rationale is that LLM is expert in reasoning while CLIP is more efficient at searching. Therefore, our framework decouples graph replanning into reasoning and searching stages, each tackled by its corresponding model. Such model collaboration reduces nodes exposure to LLM during graph distillation. Note that SayPlan assumes perfect robot execution and does not consider self-evolving action model.

## III. SYSTEM OVERVIEW

The architecture of SERP is shown Fig. 2, which consists of ASE for local replanning and GCOT for global replanning. Given a scene graph  $\mathcal{G}$  and a natural-language task instruction  $\mathcal{I}$  (e.g., "I want to play some sports"), SERP generates a sequence of executable actions  $\mathcal{A}$  fulfilling requirements (e.g., "find a basketball"). Below we present the detailed problem and system.

### A. Problem Formulation

Specifically, scene graph  $\mathcal{G} = (\mathcal{N}, \mathcal{E})$  is a hierarchical multilevel 3D representation, where  $\mathcal{N}$  and  $\mathcal{E}$  denote the sets of nodes and edges, respectively. Specifically,  $\mathcal{N}$  can be decomposed into root node, floor nodes, room nodes, and object nodes. Each node is encoded with semantic and geometric information, including object tags, spatial positions, and feature embeddings. Moreover,  $\mathcal{E}$  contains the link relationship between the nodes in  $\mathcal{N}$ . This hierarchical organization enables the  $\mathcal{G}$  to comprehensively capture both the geometrical and semantic relationships within the environment, providing a 3D memory database for LLMs.

The objective of embodied navigation is to design a planner  $\pi$  parameterized by  $\mathcal{P}$  under memory of  $\mathcal{G}$ , such that the actions  $\mathcal{A}$  fulfill task instruction  $\mathcal{I}$  under physical constraints  $\mathcal{C}$ . This is formally expressed as:  $\mathcal{A} = \pi(\mathcal{I}, \mathcal{C}|\mathcal{G}, \mathcal{P})$ . However, due to discrepancies between the constructed graph  $\mathcal{G}$  and actual scenarios, and the domain mismatch of pretrained model parameters  $\mathcal{P}$ ,  $\mathcal{A}$  may violate  $\mathcal{I}$  or  $\mathcal{C}$ . Therefore, the replanning problem is to design a function  $\varphi_\pi$  for policy  $\pi$ , so as to leverage the execution feedback for updating  $\mathcal{G}$  and  $\mathcal{P}$ :

$$[\hat{\mathcal{G}}, \hat{\mathcal{P}}] = \varphi_\pi(\mathcal{A}, \mathcal{I}, \mathcal{C}|\mathcal{G}, \mathcal{P}). \quad (1)$$

### B. Cross-level Replanning

To solve (1), this work introduces a cross-level replanning framework, i.e.,  $\varphi_\pi$  consists of two synergistic components:

(i) Global replanning module  $\varphi_G$ , which iteratively retrieves subsets of  $\hat{\mathcal{G}} \subseteq \mathcal{G}$  to see if the task can be fulfilled, as shown in the black box of Fig. 2; (ii) local replanning module  $\varphi_L$ , which iteratively updates  $\hat{\mathcal{P}} \rightarrow \mathcal{P}$  through a differentiable motion planner to prompt trajectory feasibility while adhering to kinematic constraints, as shown in the red box of Fig. 2. Accordingly, the replanning function  $\varphi_\pi$  is decomposed into

$$[\hat{\mathcal{G}}, \hat{\mathcal{P}}] = [\varphi_G(\mathcal{A}, \mathcal{I}|\mathcal{G}), \varphi_L(\mathcal{A}, \mathcal{C}|\mathcal{P})], \quad (2)$$

where  $\varphi_G$  updates  $\hat{\mathcal{G}}$  and  $\varphi_L$  updates  $\hat{\mathcal{P}}$ .

Specifically, the robot verifies actions  $\mathcal{A}$  by retrying execution and obtain  $\mathcal{F} \leftarrow \text{verify\_plan}_\pi(\mathcal{A})$ , where  $\mathcal{F}$  returns failure status and environmental contexts. Specifically, failure is reported if the agent fails to reach the destination within the time limit, exhibits prolonged stationary, or is unable to detect the target object at the planned position. If  $\mathcal{F}$  indicates failures, a local replanning phase is activated, which minimizes the following closed-loop loss function  $\mathcal{L}_{\varphi_L}$  with respect to  $\hat{\mathcal{P}}$ :

$$\varphi_L(\mathcal{A}, \mathcal{C}|\mathcal{P}) = \arg \min_{\hat{\mathcal{P}}} \mathcal{L}_{\varphi_L}(\hat{\mathcal{P}}, \mathcal{A}, \mathcal{C}|\mathcal{P}). \quad (3)$$

If local replanning fails, the global replanning phase is activated, which modifies  $\mathcal{G}$  to minimize the expected failure probability  $\mathcal{L}_{\pi_G}$  as:

$$\varphi_G(\mathcal{A}, \mathcal{I}|\mathcal{G}) = \arg \min_{\hat{\mathcal{G}}} \mathcal{L}_{\varphi_G}(\hat{\mathcal{G}}, \mathcal{A}, \mathcal{I}|\mathcal{G}). \quad (4)$$

#### IV. AGENTIC SELF-EVOLUTIONARY REPLANNING

To solve (3) and (4), there are two challenges: (i) *Effective evolution*: how to evolve improper  $\mathcal{P}$  into proper  $\hat{\mathcal{P}}$  in (3) under physical uncertainties of  $\mathcal{C}$  in test time; (ii) *Fast replanning*: the reasoning over  $\mathcal{G}$  in (4) is often computationally expensive for transformer-based LLM, which can even lead to hallucinations. Below, Sections IV-A and IV-B will present the ASE and GCOT schemes to tackle challenges (i) and (ii), respectively.

##### A. Local Agentic Self-Evolution

To begin with, we look at how illegal actions are generated. Denoting action data as  $\mathcal{A} = \{(\mathbf{a}_t, \mathbf{s}_t), \dots, (\mathbf{a}_{t+H}, \mathbf{s}_{t+H})\}$ , where  $\{\mathbf{a}_t\}$  is control sequence and  $\{\mathbf{s}_t\}$  is associated trajectory, we have  $\mathcal{A} = \arg \min_{\mathcal{A} \in \mathcal{C}} \{F(\mathcal{A})|\mathcal{P}\}$ , where the cost function over a receding horizon  $\mathcal{H} = \{t, \dots, t+H\}$  is given by [16], [24]

$$F(\mathcal{A}|\mathcal{P}) = \sum_{h=t}^{t+H} (q_s \|\mathbf{s}_h - \mathbf{s}_h^\diamond\|_2^2 + p_v \|\mathbf{e}_1^T \mathbf{a}_h - v^\diamond\|_2^2 - \eta \|\mathbf{d}_h\|_1).$$

The first item  $\|\mathbf{s}_h - \mathbf{s}_h^\diamond\|_2^2$  ensures adherence to the path plan  $\{\mathbf{s}_h^\diamond\}$ . The second item  $\|\mathbf{e}_1^T \mathbf{a}_h - v^\diamond\|_2^2$  ensures adherence to the speed plan  $v^\diamond$ . The third item  $-\|\mathbf{d}_h\|_1$  ensures safe distances from obstacles, where  $\mathbf{d}_h$  represents the distance to the closest obstacle points at time step  $h$ . The parameter set  $\mathcal{P} = \{q_s, p_v, \eta\}$  weighs the three items and controls what function to be optimized.

The reason behind fault actions  $\mathcal{A}$  is that we optimize the wrong objective function under improper  $\mathcal{P}$ . Hence, given this fault  $\mathcal{A}$ , the goal of policy  $\varphi_L$  in (3) is to find alternative  $\mathcal{P}$

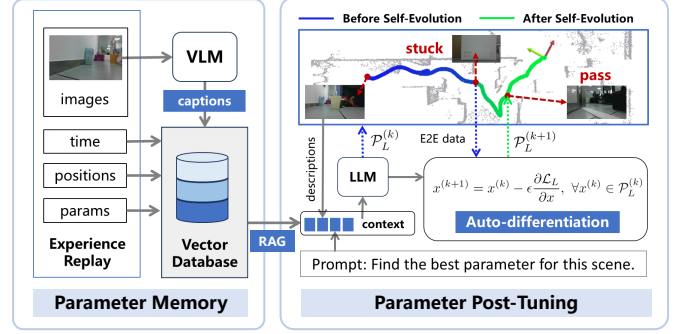


Fig. 3: Local agentic self-evolution.

and actions  $\hat{\mathcal{A}}$ , so as to execute the task without changing the global path plan  $\mathcal{S}^\diamond = \{\mathbf{s}_h^\diamond\}$  (detailed in Section IV-B).

To optimize  $\mathcal{P}$ , the self-evolution loss function is constructed according to  $F$ , which is defined as:

$$\mathcal{L}_{\varphi_L}(\hat{\mathcal{P}}) = \sum_{h=t}^{t+H} \left( \alpha \|\mathbf{s}_h(\hat{\mathcal{P}}) - \mathbf{s}_h^\diamond\|_2^2 + \beta \|\mathbf{e}_1^T \mathbf{a}_h(\hat{\mathcal{P}}) - v^\diamond\|_2^2 - \gamma \|\mathbf{d}_h(\hat{\mathcal{P}})\|_1 \right) + \omega \|\mathbf{s}_{t+H}(\hat{\mathcal{P}}) - \mathbf{s}_{\text{goal}}\|_2, \quad (5)$$

where a new item  $\omega \|\mathbf{s}_{t+H} - \mathbf{s}_{\text{goal}}\|_2$  is introduced to measure the distance between the planned state  $\mathbf{s}_{t+H}$  and the goal point  $\mathbf{s}_{\text{goal}}$ , and  $(\alpha, \beta, \gamma, \omega)$  are weight coefficients. Note that  $\{\mathbf{s}_h, \mathbf{a}_h, \mathbf{d}_h\}$  are all implicit functions of  $\mathcal{P}$ , since they are computed from oracle  $\min_{\mathcal{A} \in \mathcal{C}} \{F(\mathcal{A})|\mathcal{P}\}$ .

Given the definition of  $\mathcal{L}_{\varphi_L}$  in (5), the vanilla approach AD [16], [25] differentiates  $\hat{\mathcal{P}}$  with respect to  $\mathcal{A}$  by back propagation through the optimization problem (3). However, the landscape of  $\mathcal{A}$  over  $\mathcal{P}$  is nonconvex, making AD prone to get stuck in local optima. To mitigate this, we solve (3) using ASE, which supports “bad optima escape” by globally resetting parameters to a distant point using LLM. Moreover, AD optimizes only the parameter set  $\mathcal{P}$ , which may break down under improper  $\{\alpha, \beta, \gamma, \omega\}$ . Our ASE will jointly optimize the parameters  $\{q_s, p_v, \eta\}$  and loss weights  $\{\alpha, \beta, \gamma, \omega\}$  via ILAD. This process alternates between AD and IL: the former updates parameters based on the loss function, while the latter updates the loss function by evaluating the parameters.

Specifically, initialized with  $\mathcal{P}^{(0)}$ , at epoch  $k$  with  $k \notin \mathcal{X}$  ( $\mathcal{X}$  is a epoch set), the parameters  $\mathcal{P}^{(k)}$  are updated as

$$x^{(k+1)} = x^{(k)} - \epsilon \frac{\partial \mathcal{L}_{\varphi_L}}{\partial x}, \forall x^{(k)} \in \mathcal{P}^{(k)}, \quad (\text{AD}) \quad (6)$$

where  $\epsilon$  is the learning rate. On the other hand, if  $k \in \mathcal{X}$ , Vision-Language Model (VLM) is invoked to analyze the failure context and updating the parameters using IL as

$$\mathcal{P}^{(k+1)} = \text{VLM}(\mathcal{P}^{(k)}, \{\mathcal{A}^-, \mathcal{P}^-\}), \quad (\text{IL}) \quad (7)$$

where  $\{\mathcal{A}^-, \mathcal{P}^-\}$  denotes the execution and parameter data of previous iterations.

The above procedure is iterated until a feasible solution is attained, or the maximum local replanning epoch threshold ( $\mathcal{Y}$ ) is reached, i.e.,  $k = \mathcal{Y}$ . If no feasible solution is found, the system declares a local replanning failure, triggering the global replanning phase.

For ILAD, finding a good initial  $\mathcal{P}^{(0)}$  is of large importance.

**Algorithm 1:** SERP

---

```

1 Input: Task prompt  $\mathcal{I}$ ; Physical configuration  $\mathcal{C}$ .
2 Given: Scene graph  $\mathcal{G}$ ; Memory  $\mathcal{M}$ .
3 Retrieve  $\mathcal{P}$  from  $\mathcal{M}$   $\triangleright$  Parameter Retrieval
4 Set self-evolution counter  $k = 0$ .
5 While !timeout do
6    $\mathcal{A} = \pi(\mathcal{I}, \mathcal{C} | \mathcal{G}, \mathcal{P})$ 
7    $\mathcal{F} \leftarrow \text{verify\_plan}_{\pi}(\mathcal{A})$ 
8   If  $\mathcal{F} \neq \text{success}$  do
9     If  $k \leq \mathcal{Y} - 1$  do
10       $\triangleright$  local ASE
11      Compute  $\hat{\mathcal{P}}$  using (6) if  $k \notin \mathcal{X}$   $\triangleright$  AD
12      Compute  $\hat{\mathcal{P}}$  using (7) if  $k \in \mathcal{X}$   $\triangleright$  IL
13      Update  $\mathcal{P} \leftarrow \hat{\mathcal{P}}$ 
14       $k \leftarrow k + 1$ 
15     Else
16       $\triangleright$  global GCOT
17       $\{\mathcal{I}_1, \dots, \mathcal{I}_N\} \leftarrow \text{LLM}(\mathcal{I})$   $\triangleright$  Subtasks
18       $\hat{\mathcal{G}} \leftarrow \text{LLM}(\text{CLIP}(\mathcal{G}, \mathcal{F}, \{\mathcal{I}_1, \dots, \mathcal{I}_N\}))$   $\triangleright$  COT
19      Update  $\mathcal{G} \leftarrow \hat{\mathcal{G}}$ 
20       $k \leftarrow 0$ .
21     End If
22   End If
23 End While

```

---

To this end, we propose a retrieval augmented generation (RAG) method that pushes parameter contexts into a vector database and fetch a coarse parameter setting that roughly fits the current scene. During memorization, the robot navigates under various parameters  $\{\mathcal{P}'_1, \mathcal{P}'_2, \dots\}$ , and processes the images using vision language model, which generates a set of captions for all images. These captions are further compressed into text embeddings. Concurrently, the robot executes simultaneous localization and mapping (SLAM) to obtain a sequence of (time, pose) data frames. We use a vector database to store pairs of (time, pose, text, parameter) as a vector memory  $\mathcal{M}$ .

Conditioned on  $\mathcal{M}$ , the parameter optimization problem in (3) is thus converted into a memory-based question-answering problem, where the system needs to answer question “what is the best parameter for this scene” via memory retrieval of  $\mathcal{M}$ . The answer is formatted as a json file with keys for times, poses, texts, and parameters. This provides a coarse initial guess  $\mathcal{P}^{(0)}$  for the problem (3). Note that due to the limited memory episodes,  $\mathcal{P}^{(0)}$  is in general suboptimal to (3) under the current scene. The entire procedure of ASE is summarized in Fig. 3, which consists of parameter memorization and parameter post-tuning phases.

### B. Global Graph Chain-of-Thought

We propose GCOT for solving the global replanning problem (4). Our key insight is that for a given task  $\mathcal{I}$ , a large graph is often not required to provide a correct plan. Instead, only a subset of the graph  $\hat{\mathcal{G}} \subseteq \mathcal{G}$  is needed. Hence, the problem becomes how to find the minimum subset  $\hat{\mathcal{G}}^*$  that can fulfill  $\mathcal{I}$  given the past experience  $\mathcal{A}$ .

In practice, we cannot compute  $\hat{\mathcal{G}}^*$  and must sample  $\hat{\mathcal{G}}$ . Hence, our GCOT adopts LLM to do the sampling iteratively,

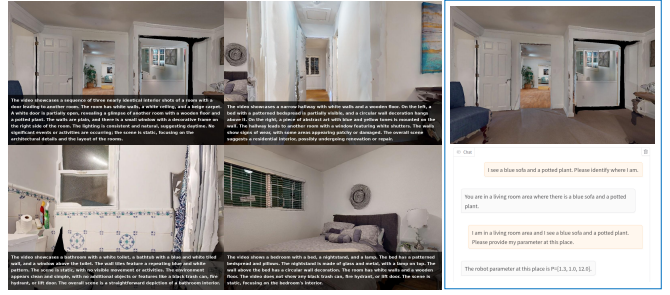


Fig. 4: Parameter retrieval in 00824.

and performs a in-context graph distillation on  $\mathcal{G}$ . The distilled graph  $\hat{\mathcal{G}}$  acts as a short-term memory that is iteratively extracted from the long-term memory  $\mathcal{G}$  for task instruction  $\mathcal{I}$  and execution experience  $\mathcal{A}$ . This dual-memory architecture enables the system to reason efficiently with critical information in  $\hat{\mathcal{G}}$ , without the need to scan all memories in  $\mathcal{G}$ .

Specifically, at each iteration, the task instruction  $\mathcal{I}$  is decomposed into  $N$  atomic sub-task  $\mathcal{I} = \{\mathcal{I}_1, \dots, \mathcal{I}_N\}$  by LLM. Feedback from previous trials is then analyzed by LLM to guide subsequent replanning. Furthermore, based on the feature extracted by CLIP model [26], a predetermined number of candidate elements are retrieved from  $\mathcal{G}$  according to the latent feature similarity via the API function `Retrieve_Element[]` for each sub-task. The semantic attributes of these candidates including object category and spatial context, are extracted using `Element_Feature[]`. Subsequently, the contextually relevant candidates selected by LLM are passed to `Element_Graph_Formation[]`, which constructs a compact task-specific graph  $\hat{\mathcal{G}}$ .

Now we consider two cases.

- If the task is not plannable with  $\hat{\mathcal{G}}$ , the LLM uses the current context and samples again to retrieve new  $\hat{\mathcal{G}}$ .
- If the task is plannable, the task plans for individual sub-tasks are generated by reasoning over  $\hat{\mathcal{G}}$ , and LLM summarizes these sub-task plans into a unified task plan.

The above process is repeated until success or timeout.

Finally, a new global path plan  $\hat{\mathcal{S}}^\diamond$  is computed by a path planner. This path  $\hat{\mathcal{S}}^\diamond$  is forwarded to the local planner, which generates new action data  $\hat{\mathcal{A}}$ . If the task is executable under  $\hat{\mathcal{A}}$ , the task succeeds. If the task is still not executable under  $\hat{\mathcal{A}}$ , the process repeats with a new  $\hat{\mathcal{G}}$  by solving (4) with  $\mathcal{A} = \hat{\mathcal{A}}$ . The entire SERP process is summarized in Algorithm 1.

## V. EXPERIMENTS AND RESULTS

We adopt the Habitat-Matterport 3D (HM3D) dataset [27] to evaluate the performance of SERP on a Ubuntu workstation with Nvidia A6000. We use scenarios [00824, 00829, 00843, 00861, 00873, 00877], with scene graphs constructed as in [9]. We also conduct real-world experiment on a car-like robot in a cluttered laboratory. SERP is compared against the following baselines: SayPlan [11], AD [15], and NeuPAN [16]. The evaluation employs the following metrics: Success weighted by inverse Path Length (SPL) [28], Success

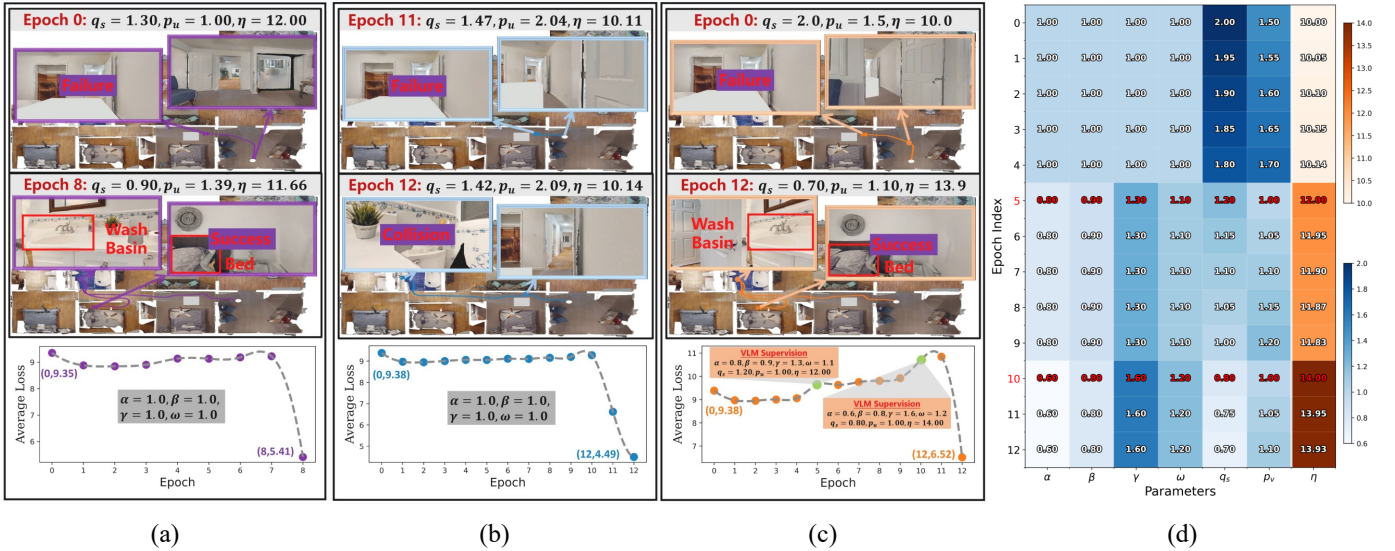


Fig. 5: Evaluation of Local replanning: (a) AD with proper RAG; (b) AD with poor RAG; (c) SERP with poor RAG; (d) parameter heatmap of (c).



Fig. 6: Global replanning results for physical failure and semantic failure.

Rate (SR), Reduced Graph Token Ratio (RGTR)<sup>1</sup>, and Mean Adaptation Epoch Count (MAEC).

### A. Qualitative Evaluations of SERP

We demonstrate the local replanning capability of SERP on the task instruction "My hands are dirty, and I only slept two hours last night." in scenario 00824, where a white box is spawned in a bedroom of Scenario 00824 to partially obstruct the initial path plan. Replanning settings are  $\mathcal{X} = \{5, 10, \dots\}$ ,  $\mathcal{Y} = 20$ , and  $\{\alpha, \beta, \gamma, \omega\} = \{1, 1, 1, 1\}$ .

First, we compare baselines with and without AD in Fig. 5a. For RAG, we adopt `qwenvl-2.5-3b` for video captioning, `fast-lio2` for SLAM, `milvus` for vector data storage, and `Nvidia remembr`<sup>2</sup> for parameter retrieval, as shown in Fig. 4. The RAG retrieves parameter  $\mathcal{P}^{(0)} = \{1.3, 1.0, 12.0\}$ . The robot gets stuck by the box, as shown on top of Fig. 5a. AD evolves  $\mathcal{P}^{(0)}$  to  $\mathcal{P}^{(8)} = \{0.90, 1.39, 11.66\}$ , which represents a reduced focus on path tracking and allows the robot to bypass the obstacle. The average evolution loss versus epoch is shown at the bottom of Fig. 5a. The loss reduction corroborates the transition from task failure to task success.

Next, we compare SERP with AD in Fig. 5b–c, under poor RAG initialization. To simulate such a case, we remove

the parameter  $\{1.3, 1.0, 12.0\}$  from the database  $\mathcal{M}$ , and the retrieved parameter becomes  $\mathcal{P}^{(0)} = \{2.0, 1.5, 10.0\}$ . In this case, AD fails as shown in Fig. 5b. The parameter is evolved to  $\{q_s, p_v, \eta\} = \{1.42, 2.09, 10.14\}$ , which helps the robot to pass the obstructed region but results in a subsequent collision. This reveals the problem with existing AD: *the evolution is highly dependent on the initial parameter provided by RAG, since its direction is limited due to its gradient descent nature*. In contrast, SERP successfully accomplishes self-evolution by utilizing ILAD as shown in Fig. 5c. At epochs 5 and 10, IL takes intervention of AD by resetting the parameters based on navigation outcomes and loss statistics. The detailed parameter heatmap during local replanning is illustrated in Fig. 5d. Notably, the IL intervention facilitates the success of AD optimization by decreasing  $(q_s, p_v)$  and  $(\alpha, \beta)$ , while increasing  $\eta$  and  $(\gamma, \omega)$ . Although the loss temporarily rises after IL intervention, representing a change of evolution direction, this results in long-term benefit towards safe navigation strategy. As a result, the robot successfully completes the task by employing the parameters obtained at epoch 12:  $\mathcal{P}^{(12)} = \{0.7, 1.1, 13.9\}$ , which demonstrates that ILAD is robust under poor RAG initialization. From this experiment, the following insight is obtained: *Unlike AD, IL enables rethinking from a whole new replanning direction, highlighting the superiority of reasoning-based tuning over gradient-only tuning*.

Finally, we evaluate local replanning with IL only. It can be

<sup>1</sup>The RGTR metric measures the reduction in token utilization required for graph information processing compared to the full scene-graph approach.

<sup>2</sup><https://github.com/NVIDIA-AI-IOT/remembr>

TABLE I: Parameter evolution using IL only.

Epoch Index	0	1	2	3	4
$q_s$	2.00	1.20	0.80	0.50	0.30
$p_v$	1.50	1.50	1.20	1.00	0.80
$\eta$	10.00	16.00	22.00	30.00	40.00

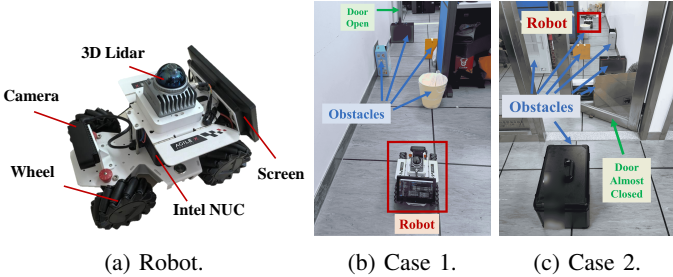


Fig. 7: Experimental setup.

seen from Table I that IL leads to value explosion of  $\eta$ , and the robot always deviates from the task plan. Indeed, VLM only provides intuitive understanding of failure rather than precise parameter adjustment. This highlights the importance of integrating both IL and AD in SERP.

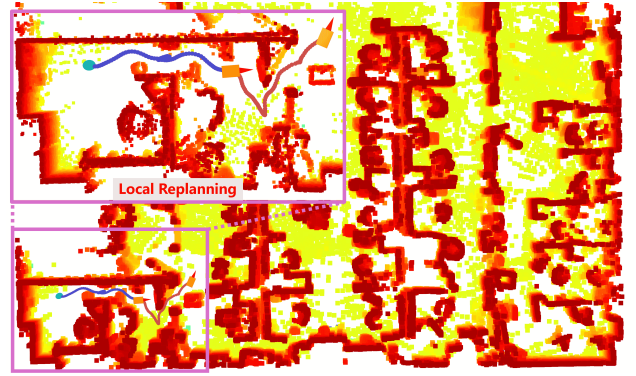
To assess the global replanning capability of SERP for physical failure, we respawn the box to completely block the path at the bedroom door in Scenario 00824. In such a case, the global replanning is activated. The task instruction is first translated to subtasks "wash hands since hands are dirty" and "rest due to lack of sleep" by GPT-4o, which are fed to CLIP for retrieving elements [[bathroom, sink], [bedroom, bed],...]. Then with the distilled graph, SERP generates an alternative path through the living room, guiding the robot turns back at the bedroom door, as shown in Fig. 6a.

To see how global replanning responds to semantic failure, inaccurate information is injected into the original scene graph by falsely including `object_0_6_32[sink_cabinet]` in `room_6[kitchen]`. As a result, the formulated task plan incorporates `object_0_6_32` in order to accomplish the first subtask. However, this step fails because the sink cabinet has been removed from the location recorded in the scene graph. Despite this failure, SERP still accomplishes the task, by forming the distilled graph and revising the task plan from `[goto(room_6[kitchen]), goto(object_0_6_32[sink_cabinet])]` to `[goto(room_6[kitchen]), goto(object_0_6_52[sink])]`, as shown in Fig. 6b.

### B. Quantitative Evaluations of SERP

This section presents quantitative evaluations to verify the efficiency and robustness of SERP. The evaluation encompasses six scenarios, each containing 15 searching tasks and 15 planning tasks, resulting in a total of 180 tasks. For every task, three trials under conditions of environmental uncertainty are conducted. To simulate environmental uncertainty, obstacles are introduced to partially or completely obstruct passages.

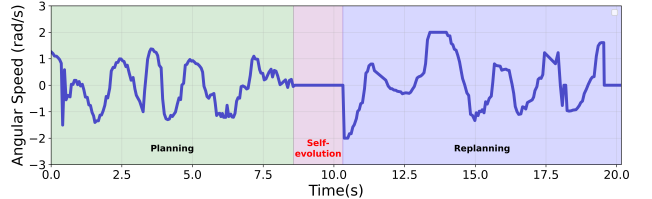
The SPL, SR and RGTR performances of SERP and SayPlan are compared in Table II. The task is regarded as success



(a) Trajectories in the point cloud.



(b) Linear speed



(c) Angular speed

Fig. 8: Trajectory and control profiles of ASE.

only upon collision-free goal attainment while fully satisfying task requirements. The results demonstrate that SERP outperforms SayPlan by over 10% SR on planning tasks. This improvement stems from the cross-level replanning mechanism of SERP, which effectively handles complex failures encountered in planning tasks. In contrast, SayPlan relies exclusively on global-level iterative replanning and often fails in scenarios that require local recovery, e.g., the robot must overcome obstacles if no alternative task plan is viable.

Furthermore, SERP achieves over 20% higher RGTR in searching task by focusing exclusively on task-relevant elements rather than task-relevant subgraph, preserving critical information while reducing token count. This performance gap increases to over 40% in planning tasks, which involve a greater number of rooms, further demonstrating the advantage of element-level selection. Note that SERP achieves slightly worse SRs than SayPlan on searching tasks in scenarios featuring a large number of objects, e.g., 00861. This is because the GCOT adopted in SERP sometimes fails in spotting the search target in the short memory. Ablation studies comparing SERP using `Qwen3-Max` versus `GPT-4o` reveal that stronger logical reasoning will enhance the task success rate.

Further evaluations assess the self-evolution capabilities of SERP against AD and VLM under improper parameter settings. We define parameter deviation as the relative difference between  $\mathcal{P}^{(0)}$  and  $\mathcal{P}^*$ , where we manually tuned  $\mathcal{P}$  exhaustively to find  $\mathcal{P}^*$ . Table III presents the SR and MAEC

TABLE II: Quantitative results of searching and planning tasks. Purple denotes the **best** performance.

Scenario		00824		00829		00843		00861		00873		00877		Avg.
Metric		SPL↑	SR↑	RGTR↑										
SayPlan [11] (Qwen3-Max)	Searching	56.1	75.6%	57.2	73.3%	56.0	77.8%	53.2	84.4%	59.8	86.7%	56.9	71.1%	75.6%
	Planning	41.3	68.9%	40.2	60.0%	43.4	71.1%	38.1	77.8%	49.3	82.2%	47.4	66.7%	53.2%
SERP (GPT-4o)	Searching	81.5	86.7%	86.5	91.1%	76.0	84.4%	65.8	75.6%	72.8	80.0%	78.5	84.4%	<b>97.0%</b>
	Planning	66.9	77.8%	75.1	84.4%	64.8	80.0%	53.4	66.7%	59.0	71.1%	70.4	80.0%	<b>93.9%</b>
SERP (Qwen3-Max)	Searching	<b>87.0</b>	<b>95.6%</b>	<b>91.0</b>	<b>97.8%</b>	<b>84.1</b>	<b>95.6%</b>	<b>75.6</b>	<b>88.9%</b>	<b>83.0</b>	<b>93.3%</b>	<b>85.1</b>	<b>95.6%</b>	95.4%
	Planning	<b>72.9</b>	<b>91.1%</b>	<b>78.4</b>	<b>95.6%</b>	<b>71.1</b>	<b>88.9%</b>	<b>64.9</b>	<b>82.2%</b>	<b>70.2</b>	<b>86.7%</b>	<b>72.9</b>	<b>88.9%</b>	90.9%

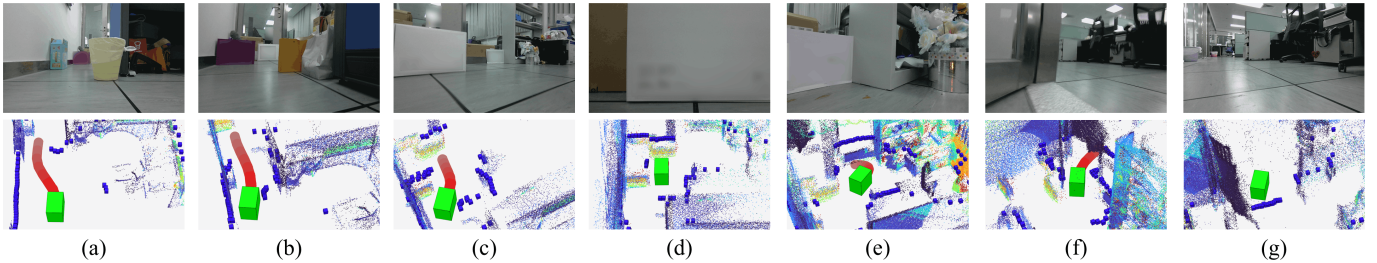


Fig. 9: Local replanning in the cluttered laboratory.

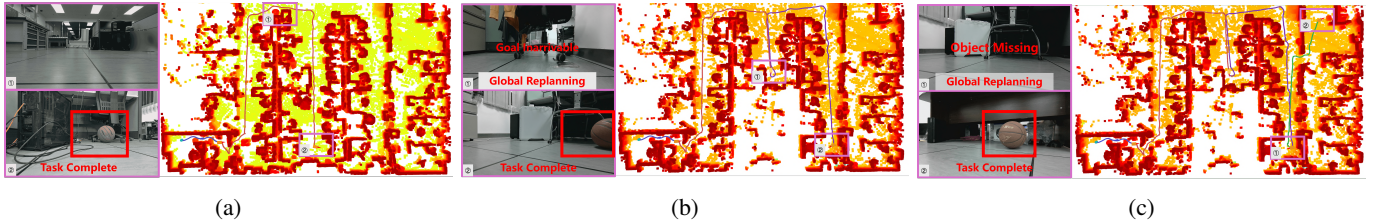


Fig. 10: Real-world testing of SERP: (a) Small door gap; (b) Unreachable goal ; (c) Missing target.

TABLE III: Comparison of SERP, AD, and VLM. Purple denotes the **best** performance.

Parameter Deviation	0%-30%		30%-60%		60%-90%	
	SR	MAEC	SR	MAEC	SR	MAEC
SERP (GPT-4o)	<b>92%</b>	<b>7.5</b>	<b>86%</b>	<b>10.6</b>	<b>58%</b>	<b>12.9</b>
AD [16]	80%	8.9	44%	14.9	16%	18.1
VLM (GPT-4o)	70%	10.2	40%	13.3	32%	15.3

for both methods, evaluated over 50 trials per parameter deviation condition. As shown in Table III, SERP achieves a 12% higher SR than AD with fewer MAEC under small parameter deviations (0%–30%). This performance gap widens substantially as deviation increases: SERP outperforms AD by over 40% with fewer MAEC.

### C. Real-World Experiment

For real-world experiment, we adopt a robot equipped with a 3D lidar, an RGBD camera, and an Intel NUC for executing the SLAM and planning packages, as illustrated in Fig. 7a. The starting position is inside an office room as shown in Fig. 7b–c. The bird’s eye view of this position in the global map is shown in Fig. 8a. The task instruction is "I want to play

some sports". Environmental uncertainties are introduced by adding obstacles and closing door (open and almost closed).

We adopt Case 1 of Fig. 7b to construct the parameter memory and test SERP in Case 2 of Fig. 7c. The robot retrieves  $\mathcal{P} = \{q_s, p_v, \eta\} = \{0.3, 0.8, 29.0\}$  from the vector database. The trajectories and control profiles of SERP are depicted in Fig. 8 and the detailed navigation process is illustrated in Fig. 9. It can be seen that the robot gets stuck in front of the door at time  $t = 8.57s$ , as shown in Fig. 8 and Fig. 9d. Upon detection of this failure, SERP performs local ASE and updates parameters to  $\mathcal{P} = \{q_s, p_v, \eta\} = \{0.12, 0.62, 29.18\}$  with 1 epoch using less than 3 seconds. At  $t = 10.32s$ , the robot successfully traverses through the narrow door, as demonstrated in Fig. 9f. After that, the robot continues to navigate for 49.36 seconds, and finds a basketball under the desk. The complete trajectory of SERP fulfilling the task is shown in Fig. 10a.

Next, we evaluate the global replanning capability of SERP by the blocking the way or moving the basketball. As shown in Fig. 10b–c, SERP is able to identify and redirect to an alternative viable goal, allowing the robot to successfully complete the task. These results demonstrate the adaptability of SERP in dynamic and uncertain scenarios.

Finally, Table IV provides ablation study to evaluate the impact of ASE. If the door is open, no matter ASE is on or off,

TABLE IV: Ablation study of ASE within SERP in real experiments.

Door	# Obstacles	Success		Navigation Time (s)		Speed Avg./Std (m/s)		Acc. Avg./Std (m/s <sup>2</sup> )	
		w/ ASE	w/o ASE	w/ ASE	w/o ASE	w/ ASE	w/o ASE	w/ ASE	w/o ASE
Open	2	✓	✓	<b>10.78</b>	11.13	<b>0.415 / 0.166</b>	0.396 / 0.179	<b>-0.028 / 1.660</b>	-0.072 / 1.978
Open	4	✓	✓	<b>10.97</b>	11.46	0.380 / 0.233	<b>0.384 / 0.189</b>	<b>-0.033 / 1.414</b>	-0.037 / <b>1.090</b>
Open	6	✓	✓	<b>11.42</b>	11.70	0.375 / 0.222	<b>0.405 / 0.180</b>	<b>-0.003 / 1.141</b>	-0.053 / 1.695
Almost Closed	2	✓	✗	<b>19.55</b>	–	<b>0.274 / 0.212</b>	–	<b>-0.024 / 1.343</b>	–
Almost Closed	4	✓	✗	<b>14.46</b>	–	<b>0.378 / 0.151</b>	–	<b>-0.020 / 1.871</b>	–
Almost Closed	6	✓	✗	<b>21.76</b>	–	<b>0.253 / 0.215</b>	–	<b>-0.028 / 2.084</b>	–

the robot is always able to navigate through the constrained region, and their average navigation times are similar (11.06s vs. 11.43s). However, in more challenging scenarios with door almost-closed, we must turn on ASE to enable the robot passing the door gap. This demonstrates the necessity of ASE in adapting internal parameters to environmental uncertainties. The average navigation time for this scenario is 18.59s.

## VI. CONCLUSION

This paper introduced SERP, a self-evolutionary cross-level replanning framework for embodied navigation. The local ASE was proposed for run-time model updates, which supports both parameter retrieval and parameter tuning. The global GCOT was designed to achieve fast optimization over large semantic and physical spaces. Thanks to these innovations, SERP can quickly recover from various failures. Extensive experiment results demonstrated that SERP outperforms existing methods, in terms of diverse metrics, and there exists mutual assistance between IL and AD.

## REFERENCES

- [1] H. Wang, W. Liang, L. V. Gool, and W. Wang, "Towards versatile embodied navigation," in *Proc. NeurIPS*, 2022, pp. 36 858–36 874.
- [2] P. Anderson, Q. Wu, D. Teney, J. Bruce, M. Johnson, N. Sünderhauf, I. Reid, S. Gould, and A. Van Den Hengel, "Vision-and-language navigation: Interpreting visually-grounded navigation instructions in real environments," in *Proc. CVPR*, 2018, pp. 3674–3683.
- [3] J. Krantz, E. Wijmans, A. Majumdar, D. Batra, and S. Lee, "Beyond the nav-graph: Vision-and-language navigation in continuous environments," in *Proc. ECCV*, 2020, pp. 104–120.
- [4] S. Chen, P.-L. Guhur, C. Schmid, and I. Laptev, "History aware multi-modal transformer for vision-and-language navigation," *Proc. NeurIPS*, vol. 34, pp. 5834–5847, 2021.
- [5] L. Ouyang, J. Wu, X. Jiang, D. Almeida, C. Wainwright, P. Mishkin, C. Zhang, S. Agarwal, K. Slama, A. Ray *et al.*, "Training language models to follow instructions with human feedback," *Proc. NeurIPS*, vol. 35, pp. 27 730–27 744, 2022.
- [6] J. Achiam, S. Adler, S. Agarwal, L. Ahmad, I. Akkaya, F. L. Aleman, D. Almeida, J. Altschmidt, S. Altman, S. Anadkat *et al.*, "Gpt-4 technical report," *arXiv preprint arXiv:2303.08774*, 2023.
- [7] D. Driess, F. Xia, M. S. Sajjadi, K. Lynch, A. Chowdhery, A. Wahid, J. Tompson, Q. Vuong, T. Yu, W. Huang *et al.*, "Palm-e: An embodied multimodal language model," 2023.
- [8] I. Armeni, Z.-Y. He, J. Gwak, A. R. Zamir, M. Fischer, J. Malik, and S. Savarese, "3d scene graph: A structure for unified semantics, 3d space, and camera," in *Proc. CVPR*, 2019, pp. 5664–5673.
- [9] A. Werby, C. Huang, M. Büchner, A. Valada, and W. Burgard, "Hierarchical Open-Vocabulary 3D Scene Graphs for Language-Grounded Robot Navigation," in *Proc. RSS*, 2024.
- [10] M. Skreta, N. Yoshikawa, S. Arellano-Rubach, Z. Ji, L. B. Kristensen, K. Darvish, A. Aspuru-Guzik, F. Shkurti, and A. Garg, "Errors are useful prompts: Instruction guided task programming with verifier-assisted iterative prompting," *arXiv preprint arXiv:2303.14100*, 2023.
- [11] K. Rana, J. Haviland, S. Garg, J. Abou-Chakra, I. Reid, and N. Sünderhauf, "Sayplan: Grounding large language models using 3d scene graphs for scalable task planning," in *Proc. CoRL*, 2023.
- [12] F. Gao, L. Wang, B. Zhou, X. Zhou, J. Pan, and S. Shen, "Teach-repeat-replan: A complete and robust system for aggressive flight in complex environments," *IEEE Trans. Robot.*, vol. 36, no. 5, pp. 1526–1545, 2020.
- [13] Z. Han, L. Xu, L. Pei, and F. Gao, "Dynamically feasible trajectory generation with optimization-embedded networks for autonomous flight," *IEEE Robot. Autom. Lett.*, vol. 10, no. 10, pp. 9995–10 002, 2025.
- [14] D. Wang, H. Ye, N. Pan, J. Huang, B. Zhang, Y. Mao, G. Huang, C. Xu, and F. Gao, "Flexible and topological consistent local replanning for multirotors," in *Proc. IROS*, 2024, pp. 5348–5355.
- [15] R. Tao, S. Cheng, X. Wang, S. Wang, and N. Hovakimyan, "Diff-tune-mpc: Closed-loop learning for model predictive control," *IEEE Robot. Autom. Lett.*, vol. 9, no. 8, pp. 7294–7301, 2024.
- [16] R. Han, S. Wang, S. Wang, Z. Zhang, J. Chen, S. Lin, C. Li, C. Xu, Y. C. Eldar, Q. Hao *et al.*, "Neupan: Direct point robot navigation with end-to-end model-based learning," *IEEE Trans. Robot.*, 2025.
- [17] S. Cheng, M. Kim, L. Song, C. Yang, Y. Jin, S. Wang, and N. Hovakimyan, "Diff-tune: Auto-tuning through auto-differentiation," *IEEE Trans. Robot.*, vol. 40, pp. 4085–4101, 2024.
- [18] J. Thomason, A. Padmakumar, J. Sinapov, N. Walker, Y. Jiang, H. Yedidion, J. Hart, P. Stone, and R. Mooney, "Jointly improving parsing and perception for natural language commands through human-robot dialog," *J. Artif. Intell. Res.*, vol. 67, pp. 327–374, 2020.
- [19] B. Bonet and H. Geffner, "Planning as heuristic search," *Artif. Intell.*, vol. 129, no. 1-2, pp. 5–33, 2001.
- [20] A. Brohan, Y. Chebotar, C. Finn, K. Hausman, A. Herzog, D. Ho, J. Ibarz, A. Irpan, E. Jang, R. Julian *et al.*, "Do as i can, not as i say: Grounding language in robotic affordances," in *Proc. CoRL*, 2023, pp. 287–318.
- [21] C. H. Song, J. Wu, C. Washington, B. M. Sadler, W.-L. Chao, and Y. Su, "Llm-planner: Few-shot grounded planning for embodied agents with large language models," in *Proc. CVPR*, 2023, pp. 2998–3009.
- [22] W. Huang, F. Xia, T. Xiao, H. Chan, J. Liang, P. Florence, A. Zeng, J. Tompson, I. Mordatch, Y. Chebotar *et al.*, "Inner monologue: Embodied reasoning through planning with language models," *arXiv preprint arXiv:2207.05608*, 2022.
- [23] B. Liu, Y. Jiang, X. Zhang, Q. Liu, S. Zhang, J. Biswas, and P. Stone, "Llm+ p: Empowering large language models with optimal planning proficiency," *arXiv preprint arXiv:2304.11477*, 2023.
- [24] X. Zhang, A. Liniger, and F. Borrelli, "Optimization-based collision avoidance," *IEEE Transactions on Control Systems Technology*, vol. 29, no. 3, pp. 972–983, 2020.
- [25] A. Agrawal, B. Amos, S. Barratt, S. Boyd, S. Diamond, and J. Z. Kolter, "Differentiable convex optimization layers," *Proc. NeurIPS*, vol. 32, 2019.
- [26] A. Radford, J. W. Kim, C. Hallacy, A. Ramesh, G. Goh, S. Agarwal, G. Sastry, A. Askell, P. Mishkin, J. Clark *et al.*, "Learning transferable visual models from natural language supervision," in *Proc. ICML*, 2021, pp. 8748–8763.
- [27] S. K. Ramakrishnan, A. Gokaslan, E. Wijmans, O. Maksymets, A. Clegg, J. M. Turner, E. Undersander, W. Galuba, A. Westbury, A. X. Chang, M. Savva, Y. Zhao, and D. Batra, "Habitat-matterport 3d dataset (HM3D): 1000 large-scale 3d environments for embodied AI," in *Proc. NeurIPS*, 2021.
- [28] P. Anderson, A. Chang, D. S. Chaplot, A. Dosovitskiy, S. Gupta, V. Koltun, J. Kosecka, J. Malik, R. Mottaghi, M. Savva *et al.*, "On evaluation of embodied navigation agents," *arXiv preprint arXiv:1807.06757*, 2018.